Results in Engineering 29 (2026) 108828

Contents lists available at ScienceDirect

Results in Engineering

journal homepage: www.sciencedirect.com/journal/results-in-engineering

Research paper

Through the surface roughness analysis and the use of silicone replicas

Andrea Genovese [a], Stefano Avolio [a,*], Andrea Ronchi [b], Antonio Serra [b], Francesco Timpone [a]

[a] Department of Industrial Engineering, University of Naples Federico II, Via Claudio, 21, Naples, 80125, Italy
[b] Pirelli Tyre S.P.A., Viale Piero e Alberto Pirelli, 25, Milano, 20126, Italy

ARTICLE INFO

Keywords:
Surface profilometry
Areal roughness
Non-destructive evaluation
Surface archiving
Texture monitoring

ABSTRACT

Direct topographic profiling of real pavement surfaces is often challenging, especially on high-traffic highways or racetracks where access time is limited. In such cases, silicone replicas offer a practical alternative for acquiring detailed surface information related to frictional behavior, wear mechanisms, and the mechanical response of materials in contact. In this work, a quantitative comparison is presented between topographic measurements carried out on two road specimens and the corresponding silicone replicas produced via dedicated molding, alongside methodological guidelines for the correct use of silicone replicas and the processing of the acquired topographic data. 3D areal parameters according to ISO 25178-2, such as the power spectral density (PSD), the probability density function (PDF), and the Abbott-Firestone curve, are compared between the silicone replica and the drill road surface to validate whether the replica can reliably reproduce the surface information. The comparison between silicone and the road specimens underlines that the technique must be employed with care, since differences attributable to "mushroom-shaped" cavities can lead to considerable errors in the roughness parameters.

1. Introduction

Surface topography plays a crucial role in tribological applications, since many functional properties such as friction, wear, lubricant retention, material fatigue, corrosion resistance, heat transfer, and optical behavior are directly linked to the shape and texture of a surface [1–3]. In the automotive sector, accurate knowledge of road roughness is essential for understanding tyre-road interactions [4–9], proving fundamental in improving road user safety.

Although areal surface-texture measurement was introduced in the manufacturing industry during the early 1980s, at that time, there was no consensus on measurement procedures or parameter selection, which led to confusion and inflated costs due to an overabundance of metrics. To address this issue, Whitehouse [10] proposed the first systematic approach for identifying the most industrially relevant parameters, and the European Community subsequently funded a collaborative research effort to further refine these guidelines [11]. The outcome was the "Birmingham Fourteen," a reduced set of three-dimensional surface-characterization parameters designed to capture the essential features of surface texture.

Since then, additional parameters were introduced to describe surface roughness more comprehensively [12,13]. Parallel efforts recast topography analysis in the frequency domain: for example, Height Difference Correlation (HDC) has been applied in the spatial domain [4,14], while Power Spectral Density (PSD) methods have been developed in the spectral domain [3,15,16]. All of these contributions ultimately informed the ISO 25178-2 [17] standard, which now defines 36 three-dimensional roughness parameters categorized as height, amplitude, spatial, hybrid, field, and feature metrics applicable to profile, image, or height-map data.

Collecting all this data is done in laboratory using high-precision profilometers, but when the object of study cannot be transported or sectioned, such as outdoor pavement, portable profilometers become necessary. Unfortunately, transporting these sensitive instruments presents several challenges:

1. Risk of damage during transit: The delicate and sensitive instruments used in topographic measurement can be easily damaged during transport, affecting their accuracy and functionality.
2. Sensitivity to environmental conditions: Devices are often susceptible to environmental changes, such as humidity, temperature fluctuations, and vibrations, which can degrade performance.
3. Security Concerns: Expensive and highly specialized equipment can pose security risks and require careful handling and secure transport arrangements to avoid theft or loss.

* Corresponding author.
E-mail addresses: andrea.genovese2@unina.it (A. Genovese), stefano.avolio@unina.it (S. Avolio), andrea.ronchi@pirelli.com (A. Ronchi), antonio.serra@pirelli.com (A. Serra), francesco.timpone@unina.it (F. Timpone).

https://doi.org/10.1016/j.rineng.2025.108828
Received 14 July 2025; Received in revised form 12 December 2025; Accepted 19 December 2025
Available online 25 December 2025

4. High logistical costs: The cost of packing, shipping, and insuring these instruments can be substantial, affecting overall project budgets.
5. Need for recalibration after transport: After transport, devices often need to be recalibrated to ensure accurate measurements, adding time and complexity to field operations.
6. Surfaces to be scanned are not always horizontal, making it impossible to place a profilometer on them.

As a practical alternative to direct in-situ scanning, one can apply silicone to create a replica of the surface. Silicone replicas are lightweight, easily transported, and storable without degradation, yet they faithfully capture fine topographic details in a matter of minutes, unlike some profilometric methods that require hours [18].

This technique has found applications across diverse fields. In dentistry, Laurent et al. [19] aimed to quantify the marginal fit of cast crowns: silicone was applied between the crown and the prepared tooth, cured, and then sectioned to provide a physical replica of the interfacial gap that could be measured under a microscope. In biomedical engineering, Doyle et al. [20] sought to manufacture patient-specific aneurysm phantoms: silicone was cast into molds reconstructed from CT scans, producing transparent vascular models for subsequent biomechanical and hemodynamic testing. In fracture mechanics, Fields and Miller [21] investigated crack initiation and crack-opening displacement; they pressed silicone onto fracture surfaces to obtain negative replicas that preserved fine topographic details for microscopic observation without altering the original specimen. In geology, Bizjak [22] characterised rock-joint roughness coefficients by pouring silicone into joint surfaces, then scanning the cured molds to extract 3D roughness descriptors relevant for geomechanical modelling.

In tribology, Persson et al. [18] explicitly questioned whether silicone replicas can reliably capture the spectral and statistical features of engineering surfaces. They emphasised that while replicas reproduce general morphology, the resolution requirements for calculating roughness indicators-particularly slope- and curvature-dependent parameters-are far more stringent than in dentistry, biomedical modelling, or geology. This raises a critical question that motivates the present study: to what extent do measurements taken on a silicone replica coincide with those obtained directly from the actual surface?

This paper aims to understand the differences between direct road measurements and silicone replicas, determining the boundaries of applicability of this indirect technique. By quantifying the approximations introduced when reconstructing roughness through silicone molds, the study identifies the precautions needed for their reliable use.

The significance of this work lies in the fact that, unlike other domains where replicas serve mainly descriptive purposes (dentistry, geology, fracture analysis), tribological and pavement applications demand quantitative fidelity of slope- and curvature-related roughness parameters. These descriptors directly feed into friction and wear models [4,6], where errors may propagate into safety-critical predictions. Furthermore, this study contributes methodologically by documenting the practical aspects of replica preparation-such as silicone type, deposition protocol, and curing times. By systematically comparing real asphalt surfaces and their replicas across multiple roughness indicators, this study fills a knowledge gap left open by previous exploratory works [18] and provides practical guidelines-including a porosity threshold-for safe and reproducible application in road engineering.

It should be noted that silicone replicas are not intended to serve as mechanical surrogates of asphalt mixtures in wear or abrasion processes. Their role is purely metrological: they provide a high-fidelity geometric record of the surface, which can be analyzed in the laboratory and used for long-term archiving. In this sense, replicas are particularly valuable for monitoring surface wear over time, as sequential molds of the same pavement location can be compared to quantify the evolution of roughness parameters under traffic and environmental loading.

In Section 2, the roughness parameters analyzed are detailed, with emphasis on the criteria employed for the choice [23]. Section 3 discusses the interpretative challenges associated with these parameters, including issues of data reduction, scale dependence, and the influence of tails. Finally, Section 4 presents the measurement results on real pavement surfaces and their silicone replicas, highlighting the key discrepancies and their implications for accurate roughness evaluation.

2. Roughness parameters

The surface's features reflect not only the manufacturing process but also the operating conditions and the mechanisms of wear it experiences. Traditional texts classify surface roughness metrics into three functional categories: amplitude, spacing, and hybrid parameters [12,13]. However, ISO 25178-2 [17] broadens this categorization by defining additional groups. In particular, beyond the amplitude, spacing, and hybrid groups, the standard introduces parameters related to areal material ratio functions, volumetric characteristics, fractal aspects, and miscellaneous surface attributes, thus offering a more comprehensive description of surface texture.

Roughness parameters can be calculated in two-dimensional (2D) form, when height values are extended along a single direction (on the Profile), or in three-dimensional (3D) form, when extended along two directions (on the Area). For this reason, these are also called Profile and Areal parameters. Since the surface analysis was born [24], a heavy use of two-dimensional profile analysis has been made in the scientific and engineering fields.

Three-dimensional parameters are now much more common because 3D areal texture analysis offers more opportunities than the study of 2D profiles [16]. However, for isotropic surfaces, the difference between the 3D and average parameters of those calculated 2D for parallel profiles is minimal [25,26]. The following discussion focuses on selected areal (3D) parameters rather than the full set of 36 defined by ISO 25178-2. Numerous studies have highlighted that many of these metrics convey overlapping information, rendering a comprehensive computation both redundant and cumbersome [23,27,28]. To address this, we have chosen a subset of parameters based on the criteria of computational simplicity, functional relevance, robustness against measurement error, and statistical independence as recommended by these authors.

2.1. Height parameters

Height parameters provide direct information on the vertical variation of the surface; they are related to the absolute value of certain heights and to the shape of the Probability Density Function (PDF).

2.1.1. Absolute peak and valley related

Among height parameters, two are related to a single value of the heights, these are: S_p (peak height), and S_v (valley depth), which are respectively the maximum and the minimum value from the mean value of the heights of the surface. These parameters are represented respectively by the Eqs. (1) and (2) and the Fig. 1.

$$S_p = max(Z(x, y)) \tag{1}$$

$$S_v = |min(Z(x, y))| \tag{2}$$

The sum of these two parameters is S_z and represents the maximum distance from the depth valley and the highest peak (Eq. (3), Fig. 1)

$$S_z = S_p + S_v \tag{3}$$

2.1.2. Heights distribution related

There are also height parameters that characterise the PDF of heights on the surface without directly specifying the heights themselves. For example, measures the spread of heights and indicates the general level

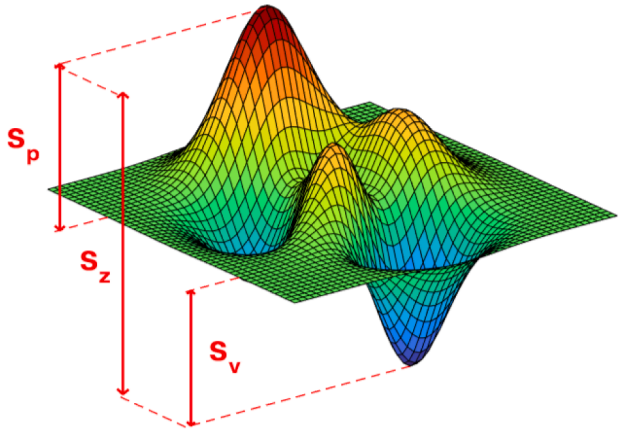

Fig. 1. Visual representation of the parameter S_p, S_v and S_z sum of the first two.

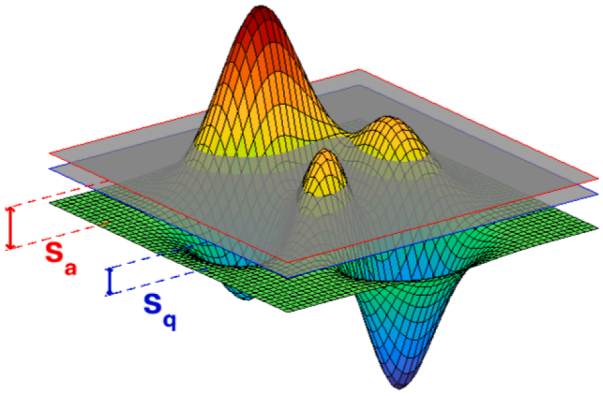

Fig. 2. Visual representation of the parameter S_a and S_q.

of roughness across the surface, and instead describes the shape of the height distribution. These parameters will be mentioned below.

S_a is the arithmetic mean of the absolute values of vertical deviation from the mean line through the surface (Eq. (4), Fig. 2).

$$S_a = \frac{1}{(m \cdot n)} \sum_{i=1}^{m} \sum_{j=1}^{n} |Z(x_i, y_j)| \tag{4}$$

Where m and n are respectively the total amount of the sampling in the direction x and y.
S_q is the Root Mean Square (RMS) value of surface heights (Eq. (5), Fig. 2).

$$S_q = \sqrt{\frac{1}{(m \cdot n)} \sum_{i=1}^{m} \sum_{j=1}^{n} Z^2(x_i, y_j)} \tag{5}$$

It is important to note that RMS coincides with the *'Standard Deviation'* because one of the initial steps in studying surfaces is to remove the mean value.

Skewness (Eq. (6), Fig. 3) and kurtosis (Eq. (7), Fig. 4), respectively S_{sk} and S_{ku}, characterise the appearance of the height distribution of the texture. Skewness gives information about the symmetry of a height distribution. A positive skewness value suggests a right-tailed height distribution, meaning deeper valleys are more likely than prominent peaks, while a negative skewness value indicates the opposite.

Kurtosis characterises the peakedness of the distribution. In surface analysis, it helps identify whether a surface exhibits pronounced peaks and deep valleys or a more uniform texture.

$$S_{sk} = \frac{1}{(m \cdot n) S_q^3} \sum_{i=1}^{m} \sum_{j=1}^{n} Z^3(x_i, y_j) \tag{6}$$

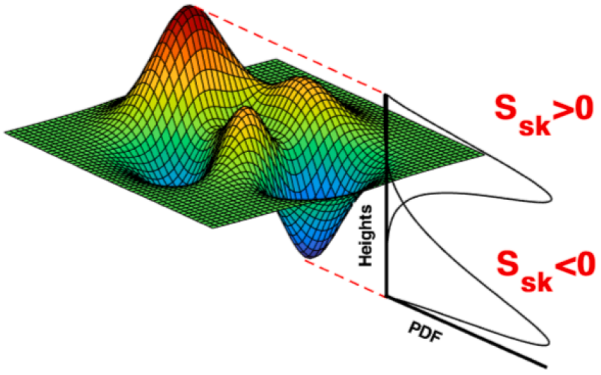

Fig. 3. Representation of what a probability density function would look like with skewness (S_{sk}) values less than and greater than zero.

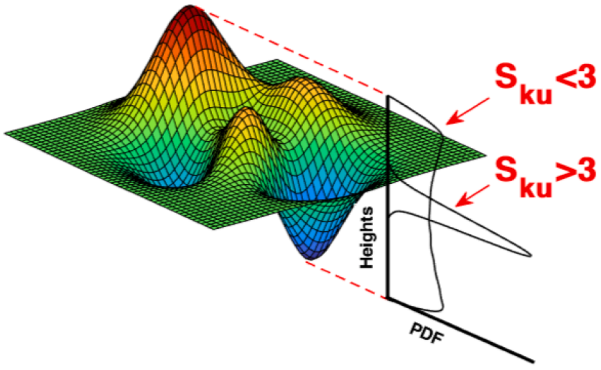

Fig. 4. Representation of what a probability density function would look like with kurtosis (S_{ku}) values less than and greater than three.

$$S_{ku} = \frac{1}{(m \cdot n) S_q^4} \sum_{i=1}^{m} \sum_{j=1}^{n} Z^4(x_i, y_j) \tag{7}$$

The reason why height distributions are important is that they are related to various tribological phenomena such as friction, wear, and lubrication. This observation is supported by research of Dzierwa et al. [29] and Sedlaček et al. [30,31], which highlighted that smooth surfaces often exhibit low friction in disk-on-sphere tests. However, the situation becomes more complex when considering rough surfaces in the dry regime. The coefficient of friction is affected by the roughness height and can vary significantly depending on the type of contact and surface conformation. In some cases, a rougher surface may increase the coefficient of friction, while in others, it may lead to increased wear and friction.

2.2. Spacing parameters

Spacing parameters quantify the spatial organization of a surface by measuring the distances between repeating features. They are derived from 3D topographical data using the Auto Correlation Function (ACF).

The ACF is an important tool in studying surface roughness. It provides information about the spatial distribution of surface height variations. Generally, autocorrelation measures how height variations at one position correlate with the same variations at other positions. If the values are highly correlated, the autocorrelation function will have higher values, whereas if the values are uncorrelated, the autocorrelation function will have values close to zero. Auto-correlation function can be calculated in both 2D and 3D, depending on the dimension of the study. 2D evaluates the correlation between height variations along a direction, while 3D auto-correlation function considers correlation in height variations across all directions of three-dimensional space.

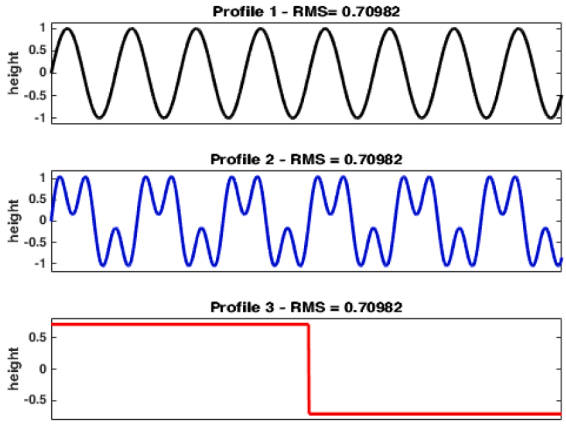

Fig. 5. Various profile with the same RMS value.

2.3. Hybrid parameters

Hybrid parameters combine amplitude and spacing. Any change in amplitude or spacing can therefore influence these parameters. The hybrid parameter and the areal interface parameter are the only two hybrid parameters contained in the ISO 25178-2 [17]. Parameter S_{dr} is also called RMS slope or surface slope. Parameter S_{dq} is the ratio of the increase in the interface area.

$$S_{dq} = \frac{1}{(M \cdot N)} \sqrt{\sum_{i=1}^{M} \sum_{j=1}^{N} \left[\left(\frac{\partial Z(x_i, y_j)}{\partial x} \right)^2 + \left(\frac{\partial Z(x_i, y_j)}{\partial y} \right)^2 \right]} \tag{8}$$

$$S_{dr} = \frac{1}{(M \cdot N)} \sum_{i=1}^{M} \sum_{j=1}^{N} \left[\sqrt{1 + \left(\frac{\partial Z(x_i, y_j)}{\partial x} \right)^2 + \left(\frac{\partial Z(x_i, y_j)}{\partial y} \right)^2} - 1 \right] \tag{9}$$

Where M and N are $m-1$ and $n-1$ respectively.

Hybrid parameters, which depend on the gradient, are greatly influenced by the sampling interval and high-frequency noise; therefore, they are often difficult to compare if measured with different instruments. It is considered that the slope (S_{dq}) is proportional to the friction coefficient between the surface and the rubber [6], or that, in general, high levels of slope can more significantly deform the rubber sliding on a surface, inducing hysteretic phenomena that are directly related to rubber friction [5,23].

3. Aspects in using roughness parameters

It has been widely noted over time that many roughness parameters present the same issues and challenges that need to be addressed. In the following sections, some of the most significant of these will be explored.

3.1. Reduction of information content and scale dependence

It has been observed that surface morphology can be described using a wide variety of parameters [32]. Indexes such as RMS, skewness, and kurtosis have been widely used to describe surfaces and the shape of their PDFs.

Unfortunately, these parameters do not adequately describe surface morphology according to Gonzalez Martinez et al. [33]. A straightforward rationale explains this phenomenon: imagine a surface represented by n × n discrete image points. If only the RMS roughness is measured, all the intricate details of the surface's structure collapse into one single numerical value. Consequently, two surfaces with distinctly different morphologies might register the same RMS roughness (Fig. 5) while exhibiting significantly different tribological behaviors.

A study conducted in 2002 by Duparre et al. [34] illustrates the difficulty in comparing roughness. The research involved measuring the surface topography of 15 samples ranging from smooth to precision-machined flat surfaces, thus covering a wide roughness range and enabling the use of various measurement techniques. When different types of measurements performed on the same samples were converted to a common quantity, such as RMS roughness, and compared, the results were generally different due to the different spatial frequency limitations of the instruments.

It has been demonstrated that the RMS roughness of a surface is dependent on the measurement scale; as the area of the image increases, the corresponding RMS value also rises. This indicates that RMS roughness is not a property that remains constant regardless of scale.

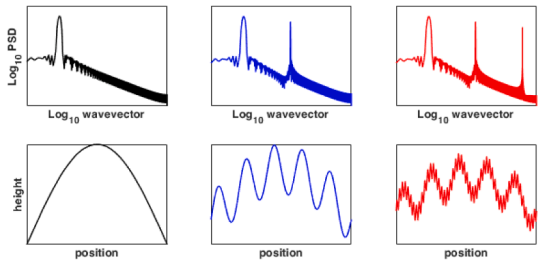

Fig. 6. The first row shows the PSD and the second row illustrates the corresponding sinusoidal composition signal.

3.2. Tails influencing

In statistical data analysis, it is crucial to consider the influence of the PDF's tails on descriptive parameters of the distribution. Long tails, which are extreme values within the dataset, can significantly distort the bell shape of the PDF and consequently affect estimates of symmetry and peakedness. For example, the presence of positive or negative long tails can alter skewness, making the distribution more or less asymmetric compared to the normal distribution [35]. Additionally, long tails can increase kurtosis, accentuating its value, even if the distribution appears Gaussian [36]. The influence of tails on these parameters can lead to misleading interpretations, as distributions with very similar shapes may exhibit significantly different skewness and kurtosis values. Therefore, it is good practice not only to consider these numerical descriptors, but also to visually inspect the shape of the distributions. When comparing two or more distributions, it is often useful to normalize and overlay them to facilitate a more accurate and meaningful comparison.

3.3. Texture wavelength

The range of texture wavelengths influences tyre-road interactions and, in turn, affects various aspects of vehicle-road dynamics, including friction, noise, and wear [37–39].

The statistical parameters described so far do not provide any information for different wavelengths. A single value will be representative of the entire surface.

For this reason, the Fourier transform of the autocorrelation function is necessary to search for something that provides information at different wavelengths, how it is possible to seen in Section 2. This tool is called *'Power Spectral Density'* (PSD) (Fig. 6).

In practice, the PSD gives information about the 'n' harmonics of the signal because the roads are made by random periodic signals. Roads are typically self-affine, where high PSD signals correspond to low wavevectors and vice versa [40].

PSD is mentioned in the ISO 25178-2 [17] as *'Fourier transformation'*. It is widely used as a road descriptor and standardized by ISO 13473-4 and 8608 [32,41]. PSD is also widely used, such as input for contact models [4,6,42] According to Jacobs et al. [40], C^{iso} is the correct form of PSD to use, as most contact models assume isotropic roughness; however, the surface should also be checked for anisotropy. For a 2D image

of the topography, this can be assessed by calculating the surface PSD C^{2D}, in which the presence or absence of radial symmetry should be evident.

It is possible to calculate the PSD^{ISO} for invariant and isotropic surfaces, which means that the statistical properties are the same on all the surface [15,40] thus it is obtained directly from the surface or the average of C_q^{1D+} [12].

It is possible to define PSD, for self-affine fractal surfaces [3], as below:

$$C^{iso}(q) = C_0 \cdot q^{(-2-2H)} \tag{10}$$

where q is the spatial wavevector while the slope of the PSD is given by $(-2-2H)$. Thus using the analytic PSD expression presented earlier, one can determine the Hurst coefficients (H).

PSD is one of the most commonly used tools for describing surfaces at different wavelengths [41,43]. However, it should be noted that PSD does not provide any information about the probability density function (PDF) of the heights, unlike S_q, S_{ku}, and S_{sk}.

4. Road & silicone comparison

This work aims to understand if there are any differences between a real road acquisition and a Silicone one and in case provide a quantitative evaluation of them.

Differences can be introduced by various factors, some related to the acquisition methodology, the type of instrument used, and repeatability, as well as the acquisition setup: scan dimensions, resolution, filters, etc [40]. Others could be due to the silicone's capability to penetrate the cavities and, therefore, replicate the surface as faithfully as possible at microscopic scales [18].

Although the present study focuses on surface replication and topographic fidelity, the implications extend directly to friction and wear modelling in pavement engineering. Reliable reconstruction of surface texture enables the evaluation of roughness parameters that influence tyre-road contact mechanics, hysteretic losses, and ultimately the friction decay that affects vehicle safety and pavement service life. By quantifying the accuracy of silicone replicas, this work provides a foundation for future applications in friction modelling, predictive maintenance, and the development of safer, longer-lasting pavement surfaces.

4.1. Experimental setup

The setup is divided into three main areas: the topography instrument, the drilling roads where the replica was performed and the silicone to make a replica.

The profilometer 'AMES 9400 HD' is a laser scanner, utilizing the laser triangulation method [44] was used to measure the surfaces to achieve statistical information of these. The instrument setup was configured to maximize the variety of samples on the acquired dimension. It acquires several equispaced lines, and for each line, it acquires a certain sampling.

In particular, as mentioned in the Section 3.1, since the RMS value, and consequently the area under the PSD, is influenced by the scan size, it would be ideal to use the largest dimension allowed by the profilometer (104x72 mm^2). However, it was necessary to reduce the size to 90x50 mm^2 due to the maximum amount of silicone that could be used for each replica.

Sha et al. [45] states that the necessary size to obtain statistical information with low variance on the surface is 50x50 mm^2. This is required to capture all the macrotexture information which, according to ISO 13473-4 [32], corresponds to wavelengths ranging from 0.5 to 50 mm, the same wavelengths that most influence friction and wear phenomena between tyre and road.

The acquisition covers a total area smaller than what is needed. In the main sampling direction, it reaches 90 mm, exceeding the minimum requirement, while in the secondary direction, it reaches 50 mm, which is still within the macrotexture range [46]. Since there are comparing scans performed with the same area and sampling, this should not pose any issue for the relative comparison.

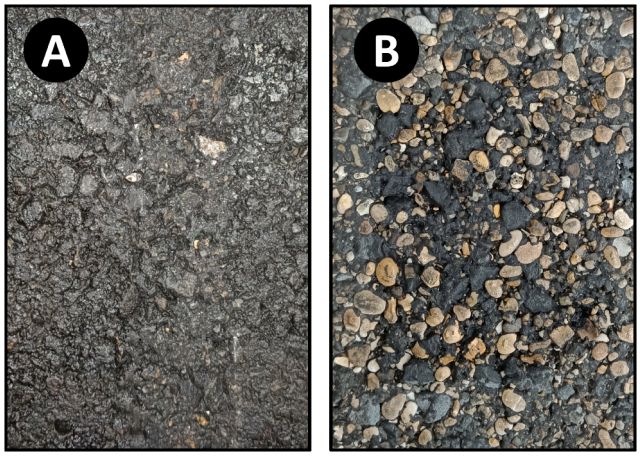

Fig. 7. Drill Road - A: Bituminous road - B: Unbituminous road.

As for the acquisition dimensions, 6.35 μm is the step between one acquired point and another, and 74.20 μm the distance between one line and another. The first was chosen to have the narrowest sampling interval of the device, while the second was set to ensure fast scanning times and quick data processing.

The two roads are drilled from real pavements, each specimen being 300x200 mm^2 in area, showing differences in aggregate size, curvature, and bitumen distribution (Fig. 7). For simplicity, these are referred to as 'Road A' and 'Road B'.

It should be noted that no information was available regarding the mix design or volumetric properties of the materials (aggregate gradation, bitumen content, porosity). This is consistent with the practical context of the study, which aims to investigate surface topography as retrieved from real pavements, such as racing tracks, where such material properties are typically unknown or inaccessible. Scans were performed on these roads with the same instrument setup, and, in the same scanning area, a silicone mold was also made using a widely employed silicone for non-destructive replication in material testing.

A two-component fast-curing silicone rubber was employed to obtain non-destructive replicas of the asphalt surface. The cured replicas reproduce fine features down to approximately 0.1 μm, with negligible shrinkage and a tear strength in the order of 15-20 kN/m^2. The material exhibits a viscosity of about 18,000 mm^2/s at 25 °C and cures within 10-15 min under ambient conditions. Once cured, the replicas are dimensionally stable over time, allowing for long-term storage and subsequent laboratory analysis. Similar silicone compounds are widely used in the dental field for impression techniques, where their cost is on the order of 10 € per 100 g, making them affordable also for field applications in pavement engineering.

A template with a 100x60 mm^2 hole was used for the application of silicone via mixing Handgun. Ensuring the spread in a specific area, where subsequently the topography is measured.

The measure of the actual road and its replica presents the same asperity and Hill/Cave (respectively the opposite due to the silicone being the replica of the road,) Fig. 8.

Regarding durability, once cured, the silicone replicas remain dimensionally stable over time and can be reused for repeated profilometric analyses without measurable degradation. Based on laboratory experience and manufacturer data, replicas can be stored for years if kept in dry, dust-free environments and protected from direct sunlight or high temperatures. However, the material is not intended for mechanical loading or friction testing, and each replica should be used solely for topographic measurements.

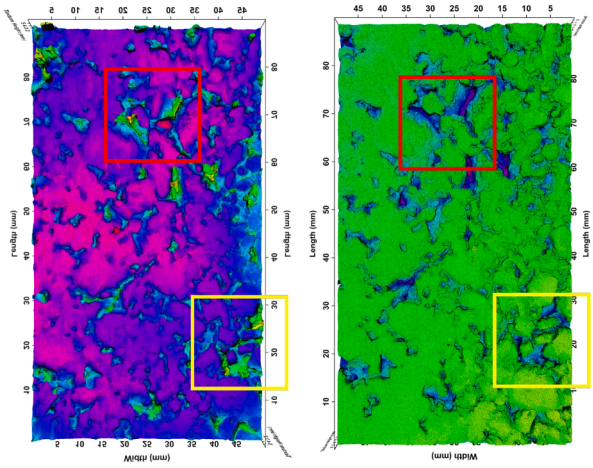

Fig. 8. Silicone (left) and road (right) measurements and their similarities.

Table 1
Descriptors A.

Road A	Sp (m)	Sv (m)	Sz(m)	S_a (m)	S_q (m)	S_{ku}	S_{sk}	S_{dq}	S_{dr}
Road	11.82e-4	39.21e-4	51.03e-4	3.47e-4	4.95e-4	8.77	−2.17	2.76	0.64
Silicone	14.01e-4	36.08e-4	50.09e-4	4.10e-4	5.59e-4	6.44	−1.61	3.15	0.49
Error %	18.53	−7.98	−1.84	18.16	12.93	−26.57	25.81	14.13	−23.44

Table 2
Hurst coefficients.

Road A	Hurst
Drill	0.659
Silicone	0.660
Error %	0.15

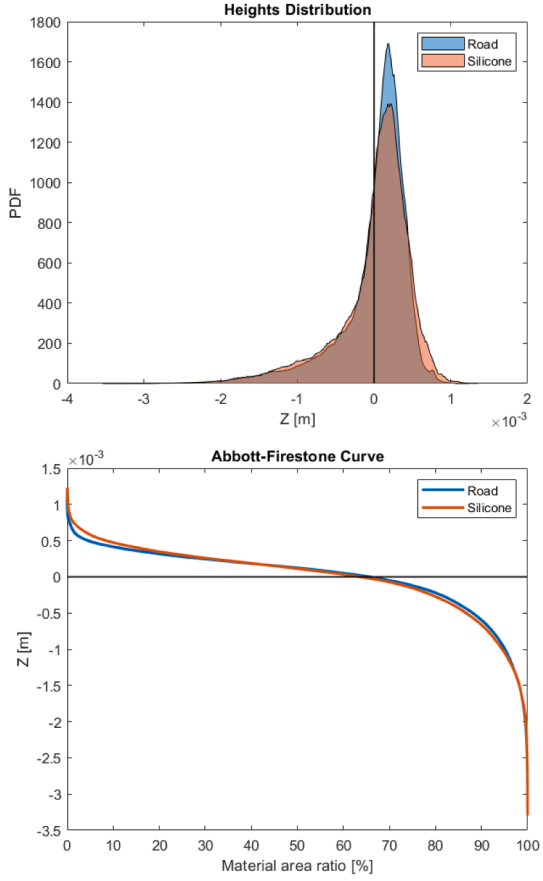

Fig. 9. PDF and Abbott-Firestone curve for road A and its silicone replica.

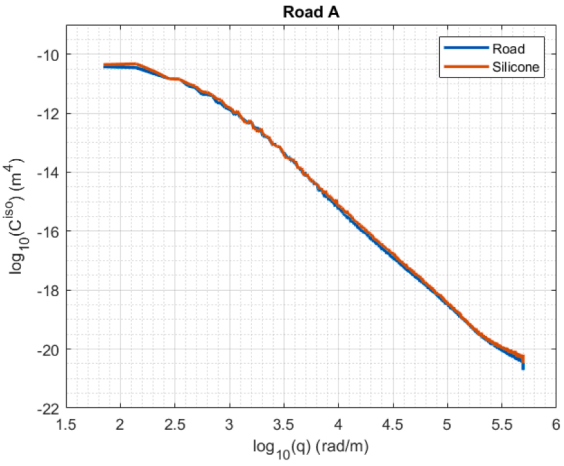

Fig. 10. C^{iso} comparison between roads A and its silicone replica.

4.2. Results & discussion

Below, the road descriptors seen previously will be examined and commented on, calculated for both roads and their respective silicone mold. Results will be presented in terms of: S_p, S_v, S_z, S_a, S_q, S_{ku}, S_{sk}, S_{dq}, S_{dr} and PSD. The Hurst coefficient (H) will also be reported to emphasize the differences in the PSDs.

4.2.1. Road A

Height Parameters related to absolute peak and valley: S_p, S_v, S_z have an absolute error ranging from 1.84 to 18.53%. S_z has the lowest error and this means that the relative value among the maximum and minimum height is maintained.

Height Parameters related to the height distribution S_a, S_q, S_{ku} and S_{sk} have an absolute error ranging from 12.93 to 26.57%. The errors of the first two parameters are in the range of the parameters related to absolute peak and valley. However, it is possible to see that values like S_{ku} and S_{sk} tend to have a larger error, particularly as they move towards normalizing the height distributions. Kurtosis will tend to 3 and Skewness will tend to 0.

Probability Density Function is connected to parameters how S_{ku} and S_{sk}, but as mentioned in paragraph Section 3.2, these parameters are influenced by the tails of the height distribution (Tables 1, 2), It is possible to notice an error around 25% for both, but it is also possible to see from Fig. 9 that the height distribution and the material ratio are quite the same for road and silicone.

Hybrid Parameters: S_{dq} and S_{dr} have an absolute error in the range of the other parameters, in complete agreement with the other indexes. Silicone effectively captures the frequency content of Road A, as demonstrated by the strong similarity between the PSD curves of the original surface and its replica, with a Hurst coefficient error of 0.15% of the silicone from the real road.

Characteristic curves such as the PDF, Abbott-Firestone curve, and PSD (Figs. 9–10) appear significantly more similar between the silicone replica and the actual road than do the statistical parameters. This occurs because the PDF and Abbott-Firestone curves illustrate, even qualitatively, the magnitude and cumulative distribution of heights recorded by the profilometer, rendering them unaffected by the issues outlined in Section 3. The PSD, being independent of absolute height values and their distribution, considers only the frequency content of the surfaces, allowing the curves of the road and the silicone replica to overlap.

Table 3
Descriptors B.

Road B	$Sp\ (m)$	$Sv\ (m)$	Sz(m)	$S_a\ (m)$	$S_q\ (m)$	S_{ku}	S_{sk}	S_{dq}	S_{dr}
Road	22.80e-4	31.82e-4	54.62e-4	4.69e-4	6.06e-4	4.57	−1.34	2.50	0.57
Silicone	22.55e-4	53.16e-4	75.62e-4	7.56e-4	9.78e-4	4.71	−1.40	6.27	0.85
Error %	−1.10	67.07	38.45	61.19	61.39	3.06	−4.8	150.8	49.12

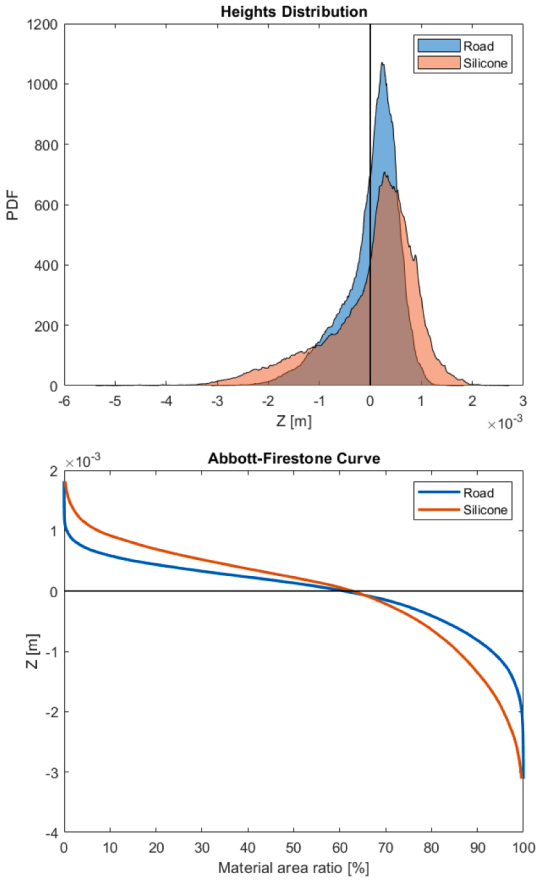

Fig. 11. PDF and Abbott-Firestone curve for road B and its silicone replica.

4.2.2. Road B

Height Parameters related to absolute peak and valley: S_p, S_v, S_z have an absolute error ranging from 1.84 to 18.53%. If the lowest value is smaller than the road A, the error for the value S_z is much higher than the road A.

The trend of the Height Parameters related to the height distribution is the opposite of the Road A. The absolute error for S_a, S_q is higher than S_{ku} and S_{sk}. This seams to be that the Probability Density function is well replicate by the silicone, but also for this road the tails of the height distribution have a large impact on the values like S_{ku} and S_{sk}, which even if the absolute error is in the range of around 3/5% but it is possible to see a big different in terms of distribution and the material ratio in Fig. 11.

It is worth noting that S_{dq} and S_{dr} exhibit the largest discrepancies between road and replica (Tables 3, 4). This effect does not originate from the molding fidelity, but from the way the replica is subsequently scanned: while the silicone reproduces the geometry with high accuracy, the optical profilometer interacts differently with the replica than with the real asphalt, especially in correspondence with cavities and undercut features. As a result, descriptors related to local gradients and developed area are particularly affected (explanation in Section 4.3.)

In addition, the replica of Road B fails to reproduce the spectral content of the surface. The PSD (Fig. 12) shows an upward shift and the

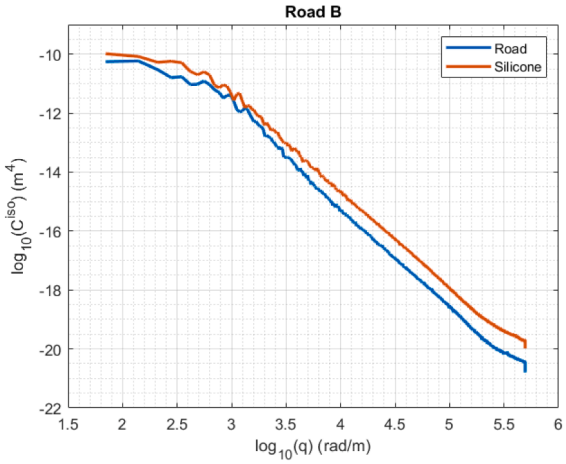

Fig. 12. C^{iso} comparison between roads B and its silicone replica.

Table 4
Hurst coefficients.

Road B	Hurst
Drill	0.681
Silicone	0.632
Error %	−7.20

Hurst coefficient deviates with an absolute error of 7.2%. These spectral differences confirm that, for Road B, silicone replicas do not provide reliable information on the actual pavement.

This divergence is also visible in the probability and material ratio curves (Fig. 11), where the distributions from silicone clearly depart from those of the real surface, producing large errors in statistical parameters. In contrast, for Road A, such discrepancies are negligible: compactness of aggregate particles fills the voids and prevents the formation of undercut cavities, allowing the silicone to replicate the same topography that the laser scanner detects directly. All of these observations are consistent with the surface phenomena that will be explained in detail in the following subsection.

4.3. Mushroom aspects

There are significant differences in the roughness parameters between roads and replicas more significant on the road B than on the A. This is because roads present a large amount of space in the cavities below the top plane. This means that the topography measurements on the silicone replica of these roads are affected by an intrinsic error since the shape of the silicone does not reflect what the profilometer acquires from above.

During the molding process, the silicone infiltrates the gaps between the pebbles, ensuring that these voids are faithfully replicated. Notably, the resulting silicone mold captures the distinctive *mushroom-shaped* cavities from the original surface. (Fig. 13).

This phenomenon impacts the measurement of the replica because the laser projects onto the surface along its line of sight, failing to capture recessed areas that are not directly visible. A graphical depiction of this effect is provided in Fig. 14, where the coupling of road-silicone is shown and Fig. 15, where the acquisition process of both road and silicone is shown [47].

This effect can be interpreted as a combination of transient phenomena and boundary effects. During the replication process, the silicone mold deforms around the road asperities, especially at their edges. These boundary regions, where the transition between peak and valley occurs, tend to be exaggerated. As a result, the replica includes exaggerated valleys that do not correspond to the actual road profile.

Fig. 13. Mushroom shape on silicone mold.

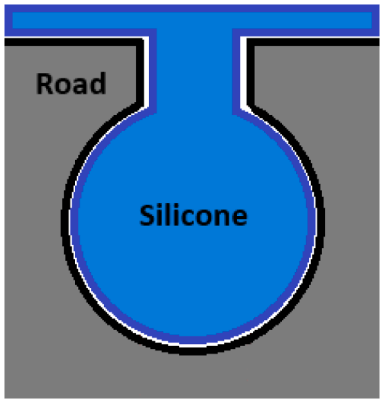

Fig. 14. Schematic proof of silicone mushroom replica.

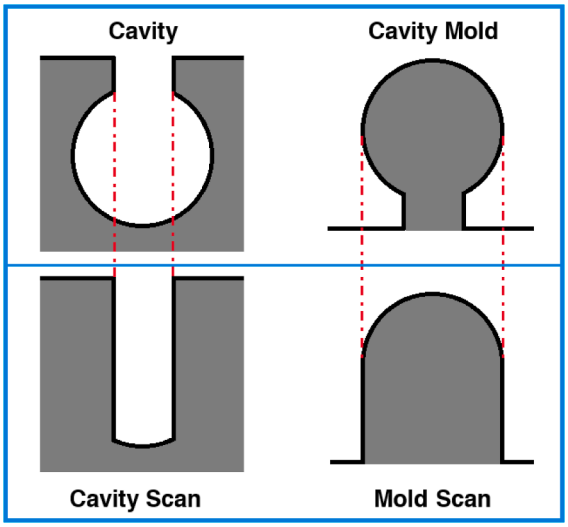

Fig. 15. Measurement phenomenon and boundary effects.

Moreover, during the laser scanning phase, the beam can only detect surfaces within its direct line of sight. This creates a shadowing effect, especially in steep or undercut regions, where the laser cannot penetrate. These transient visibility conditions result in an incomplete acquisition of the mold, underestimating peaks and overestimating valleys.

Mushroom-like shapes, as shown in Fig. 13, represent the reverse of the cavities (valleys) of the actual road surface. As a result, silicone molds of roads with a lack of bitumen in the cavities tend to replicate larger valleys than those detectable by the laser scanner from above, precisely due to silicone that expands into the empty spaces (causing a mushroom shape). While the number of peak heights may be preserved, the size of the cavities is significantly distorted, leading to substantial errors in the roughness parameters.

It is therefore deducible that surfaces with low porosity are more suitable for the use of silicone replicas to obtain statistical information, such as sandpaper, corundum, metals, and ceramics.

5. Conclusions

The comparative analysis between direct asphalt measurements and silicone replicas has revealed clear differences in replication fidelity. Road A, characterized by bitumen covering the aggregate interstices, showed a good agreement between real and replicated surfaces. In contrast, Road B, lacking bitumen at the aggregate boundaries, exhibited pronounced discrepancies. The presence of deep cavities and voids that could not be properly filled during molding led to the formation of “mushroom-shaped” protrusions, which altered the replicated topography.

These structural differences translated into significant errors in several roughness descriptors. Amplitude-related parameters such as S_a and S_q remained relatively stable, while slope- and curvature-dependent metrics (S_{dq}, S_{dr}) were strongly affected because strongly connected with the slope of the PSD [3]. Spectral analyses confirmed these findings, with an upward shift in the PSD and notable errors in the Hurst coefficient. Although distribution parameters like skewness and kurtosis appeared less sensitive, their values were still influenced by the tails of the height distribution.

From a mechanical standpoint, silicone and asphalt mixtures exhibit fundamentally different elastic and viscoelastic properties. The elastic modulus of cured silicone rubber typically ranges between 1 and 10 MPa, while that of asphalt mixtures, dominated by the aggregate skeleton, is in the order of several GPa. This disparity of more than three orders of magnitude means that silicone cannot reproduce the stress distribution, local deformation, or micro-fracture mechanisms occurring under real traffic loads. Consequently, replicas can only be used for geometric monitoring of surface evolution and not for reproducing the mechanical wear mechanisms themselves.

From an application perspective, the results suggest that silicone replicas can be a valuable non-destructive tool when applied to dense asphalt surfaces with low porosity, such as conventional wearing courses and racetrack pavements. In these cases, replicas reproduce most roughness descriptors with acceptable errors and allow reliable monitoring of surface wear and polishing. Conversely, in highly porous mixtures such as open-graded friction courses and drainage asphalts, the presence of interconnected voids leads to systematic distortions that strongly affect slope-related parameters and spectral indicators, limiting the reliability of replicas for advanced roughness evaluation.

This methodological boundary is highly relevant for skid resistance studies: surface wear and polishing are among the main drivers of friction decay, as demonstrated in several recent investigations on asphalt pavements that correlated the evolution of 3D texture parameters with skid resistance performance [48–50]. In this context, silicone replicas offer a practical means to capture and archive surface conditions, enabling longitudinal monitoring of polishing effects without the need for invasive core sampling. This makes the method especially useful for laboratory-based investigations of friction decay and for comparative studies across different pavement types, provided that porosity remains below a certain threshold.

In summary, this study demonstrates that silicone replicas are reliable when applied to dense, low-porosity asphalt mixtures, where they reproduce amplitude-type roughness descriptors and material ratio curves with acceptable accuracy. In contrast, replicas of highly porous or open-graded mixtures are affected by void-induced artefacts that compromise slope-related and spectral parameters. These findings establish the conditions under which replicas can be confidently used, while also delineating their intrinsic limitations.

CRediT authorship contribution statement

Andrea Genovese: Writing – review & editing, Supervision, Project administration, Methodology, Formal analysis, Conceptualization; **Stefano Avolio:** Data curation, Formal analysis, Methodology, Software, Validation, Visualization, Writing – original draft; **Andrea Ronchi:** Writing – review & editing, Validation, Software, Resources, Methodology, Investigation, Data curation; **Antonio Serra:** Validation, Software, Resources, Methodology, Investigation, Conceptualization; **Francesco Timpone:** Writing – original draft, Visualization, Supervision, Resources, Formal analysis.

Data availability

The data that has been used is confidential.

Declaration of competing interest

The authors declare that they have no known competing financial interests or personal relationships that could have appeared to influence the work reported in this paper.

References

[1] J.R. Barber, Contact Mechanics, 20, Springer, 2018.
[2] P. Pawlus, R. Reizer, M. Wieczorowski, Characterization of the shape of height distribution of two-process profile, Measurement 153 (2020) 107387.
[3] B.N.J. Persson, Contact mechanics for randomly rough surfaces, Surf. Sci. Rep. 61 (4) (2006) 201–227.
[4] M. Kluppel, G. Heinrich, Rubber friction on self-affine road tracks, Rubber Chem. Technol. 73 (4) (2000) 578–606.
[5] K.A. Grosch, The relation between the friction and visco-elastic properties of rubber, Proc. R. Soc. London. Ser. A. Math. Phys. Sci. 274 (1356) (1963) 21–39.
[6] B.N.J. Persson, Theory of rubber friction and contact mechanics, J. Chem. Phys. 115 (8) (2001) 3840–3861.
[7] F. Farroni, R. Russo, F. Timpone, Experimental investigations on rubber friction coefficient dependence on visco-elastic characteristics, track roughness, contact force, and slide velocity, Tire Sci. Technol. 45 (1) (2017) 3–24.
[8] V.M. Arricale, A. Sammartino, G. Napolitano Dell'Annunziata, F. Timpone, RIDElab: advanced calibration tool for a real-time MF-based multiphysical tire model, AIP Publishing 2872 (1) (2023).
[9] V.M. Arricale, A. Genovese, F. Farroni, A. Maiorano, L. Mosconi, A. Sakhnevych, F. Timpone, Experimental friction analysis through innovative compound-substrate contact modeling for automotive applications, AIP Publishing 2872 (1) (2023).
[10] D.J. Whitehouse, The parameter rash-is there a cure? Wear 83 (1) (1982) 75–78.
[11] K.J. Stout, The development of methods for the characterisation of roughness in three dimensions, EUR 15178 EN of Commission of the European Communities 358 (1994).
[12] E.S. Gadelmawla, M.M. Koura, T.M.A. Maksoud, I.M. Elewa, H.H. Soliman, Roughness parameters, J. Mater. Process. Technol. 123 (1) (2002) 133–145.
[13] B. Bhushan, Surface roughness analysis and measurement techniques, Modern Tribology Handbook, Two Volume Set (2000) 79–150.
[14] A. Lang, M. Klüppel, Influences of temperature and load on the dry friction behaviour of tire tread compounds in contact with rough granite, Wear 380 (2017) 15–25.
[15] B. Persson, On the fractal dimension of rough surfaces, Tribol. Lett. 54 (2014) 99–106.
[16] B.N.J. Persson, Contact mechanics for randomly rough surfaces: on the validity of the method of reduction of dimensionality, Tribol. Lett. 58 (2015) 1–4.
[17] I.O.f. Standardization, ISO 25178: Geometrical product specifications (GPS) - surface texture: Areal - Part 2: terms, definitions and surface texture parameters, 2021, (International Organization for Standardization).
[18] J.S. Persson, A. Tiwari, E. Valbahs, T.V. Tolpekina, B.N.J. Persson, On the use of silicon rubber replica for surface topography studies, Tribol. Lett. 66 (2018). https://doi.org/10.1007/s11249-018-1092-0
[19] M. Laurent, P. Scheer, J. Dejou, G. Laborde, Clinical evaluation of the marginal fit of cast crowns–validation of the silicone replica method, J. Oral. Rehabil. 35 (2) (2008) 116–122.
[20] B.J. Doyle, L.G. Morris, A. Callanan, P. Kelly, D.A. Vorp, T.M. McGloughlin, 3D reconstruction and manufacture of real abdominal aortic aneurysms: from CT scan to silicone model, ASME. J. Biomech. Eng. (2008); 130 (3): 034501
[21] B.A. Fields, K.J. Miller, A study of COD and crack initiation by a replication technique, Eng. Fract. Mech. 9 (1) (1977) 137–146.
[22] K.F. Bizjak, Determining the surface roughness coefficient by 3D scanner, Geologija 53 (2) (2010) 147–152.
[23] P. Pawlus, R. Reizer, M. Wieczorowski, Functional importance of surface texture parameters, Materials 14 (18) (2021) 5326.
[24] E.J. Abbott, S. Bousky, D.E. Williamson, The profilometer, Mech. Eng. 60 (3) (1938) 205–216.
[25] T. Tsukada, T. Kanada, Evaluation of two-and three-dimensional surface roughness profiles and their confidence, Wear 109 (1-4) (1986) 69–78.
[26] R. Ohlsson, B.G. Rosén, J. Westberg, The interrelationship of 3D surface characterisation techniques with standardised 2D techniques, Advanced Techniques for Assessment Surface Topography Development of a basis for 3D surface texture standards "surfstand". West Sussex: Kogan Page Science (2003) 197–220.
[27] R. Deltombe, K.J. Kubiak, M. Bigerelle, How to select the most relevant 3D roughness parameters of a surface, Scanning J. Scanning Microscopies 36 (1) (2014) 150–160.
[28] D.J. Whitehouse, Handbook of Surface and Nanometrology, Taylor & Francis, 2002.
[29] A. Dzierwa, P. Pawlus, W. Zelasko, R. Reizer, The study of the tribological properties of one-process and two-process textures after vapour blasting and lapping using pin-on-disc tests, Key Eng. Mater. 527 (2013) 217–222.
[30] M. Sedlaček, B. Podgornik, J. Vižintin, Influence of surface preparation on roughness parameters, friction and wear, Wear 266 (3-4) (2009) 482–487.
[31] M. Sedlaček, B. Podgornik, J. Vižintin, Correlation between standard roughness parameters skewness and kurtosis and tribological behaviour of contact surfaces, Tribol. Int. 48 (2012) 102–112.
[32] I.O.f. Standardization, ISO 13473: Characterization of pavement texture by use of surface profiles - Part 4: one third octave band spectral analysis of surface profiles, 2024, (International Organization for Standardization).
[33] J.F. González Martínez, I. Nieto-Carvajal, J. Abad, J. Colchero, Nanoscale measurement of the power spectral density of surface roughness: how to solve a difficult experimental challenge, Nanoscale Res. Lett. 7 (2012) 1–11.
[34] A. Duparre, J. Ferre-Borrull, S. Gliech, G. Notni, J. Steinert, J.M. Bennett, Surface characterization techniques for determining the root-mean-square roughness and power spectral densities of optical components, Appl. Opt. 41 (1) (2002) 154–171.
[35] G. Brys, M. Hubert, A. Struyf, A robust measure of skewness, J. Comput. Graphical Stat. 13 (4) (2004) 996–1017.
[36] R.A. Maronna, R.D. Martin, V.J. Yohai, M. Salibián-Barrera, Robust Statistics: Theory and Methods (with R), John Wiley & Sons, 2019.
[37] J.J. Henry, Evaluation of Pavement Friction Characteristics, 291, Transportation Research Board, 2000.
[38] N.Z. Garcia, J.A. Prozzi, Contribution of Micro-And Macro-Texture for Predicting Friction on Pavement Surfaces, Technical Report, 2016.
[39] N.Z. Garcia, Predicting Friction with Improved Texture Characterization, Ph.D. thesis, University of Texas, 2017.
[40] T.D.B. Jacobs, T. Junge, L. Pastewka, Quantitative characterization of surface topography using spectral analysis, Surf. Topogr. Metrol. Prop. 5 (1) (2017) 013001.
[41] I.O.f. Standardization, ISO 8608: mechanical vibration - road surface profiles - reporting of measured data, 2016, (International Organization for Standardization).
[42] M.H. Müser, W.B. Dapp, R. Bugnicourt, P. Sainsot, N. Lesaffre, T.A. Lubrecht, B.N.J. Persson, K. Harris, A. Bennett, K. Schulze, et al., Meeting the contact-mechanics challenge, Tribol. Lett. 65 (2017) 1–18.
[43] P. Andren, Power spectral density approximations of longitudinal road profiles, Int. J. Veh. Des. 40 (1-3) (2006) 2–14.
[44] A. Engineering, AMES Engineering Laser Texture Scanner - Software User Manual, 2020.
[45] A. Sha, D. Yun, L. Hu, C. Tang, Influence of sampling interval and evaluation area on the three-dimensional pavement parameters, Road Mater. Pavement Des. 22 (9) (2021) 1964–1985.
[46] M. Mahboob Kanafi, A. Kuosmanen, T.K. Pellinen, A.J. Tuononen, Macro-and microtexture evolution of road pavements and correlation with friction, Int. J. Pavement Eng. 16 (2) (2015) 168–179.
[47] S. Avolio, E. Lenzi, G.N. Dell'Annunziata, M. Ruffini, A. Genovese, Topography measurements analysis between road surfaces and their silicone replicas, in: International Tribology Symposium of IFToMM, Springer, 2024, pp. 357–366.
[48] Y. YAN, et al., Research on skid resistance performance of asphalt pavement based on 3D texture feature parameters (2024).
[49] L. Junjie, W. Hong, G. Rongxin, B. Lingchen, L. Binjin, H. Kaiyong, Z. Bin, Y. Feng, Study on the skid resistance decay of submerged asphalt pavements based on texture parameters, Mater. Struct. 57 (10) (2024) 223.
[50] W. Ren, J. Li, Y. Zhang, X. Wang, R. Shao, Road surface texture evaluation and relation to low-speed skid resistance for different types of mixtures, Coatings 14 (11) (2024) 1367.